



OPEN

Spin-Hall conductivity and Hall angle in a two-dimensional system with impurities in the presence of spin-orbit interactions

Hemant Kumar Sharma¹, Shreekantha Sil² & Ashok Chatterjee¹✉

We investigate the spin-torque-dependent Spin Hall phenomenon in a two-dimensional tight-binding system in the presence of Rashba and Dresselhaus spin-orbit interactions and random static impurities. We employ the Matsubara Green function techniques to calculate the relaxation time caused by the scattering of electrons by impurities. The longitudinal and transverse conductivities are next calculated with the help of the Kubo formalism. We have also calculated the spin Hall angle for the present model and studied its dependence on spin-orbit interactions and impurity strength. Finally, we explore the effect of interplay between the Rashba and Dresselhaus interactions on the spin-Hall effect.

With recent development in the field of spin-based devices, the subject of Spintronics has become an active area of research in low-dimensional physics for its potential applications in spin filters, field-effect spin transistors, information processing, and mass storage^{1,2}, magnetic recording, sensors and so on. Spin transport plays a key role in spintronic devices and causes a spin current in a similar manner the charge transport gives the charge current. Methods like injecting ferromagnetic atoms in a non-ferromagnetic material^{3–10} have been used widely in the past to get spin current. However, this method is efficacious only when the magnetic field is strong. An alternative approach has been proposed by Sharma et al.¹¹ to produce spin current in the GaAs/AlGaAs hetero-structure. Here the basic idea is that in the GaAs/AlGaAs hetero-structure cavity, the spin-orbit interaction couples the electron's spin and orbital motion making the electrons of the system spin-polarized¹¹. The study of intrinsic Spin-Hall effect in p-doped semiconductors by Murakami et al.¹² and in a two-dimensional (2D) electron gas by Sinova et al.¹³ with a substantial Rashba spin-orbit coupling has brought the subject of spintronics to the forefront of current research. The intrinsic spin-Hall effect refers to a non-dissipative spin current flowing normal to the driving electric field when the spin-orbit interaction (SOI) dominates over the quantum collisions caused by the disorder. This is in contrast to the extrinsic Spin-Hall effect proposed by Hirsch¹⁴ and Zhang¹⁵, where the spin current is generated by the spin-orbit dependent scattering from the impurity. Also, the effect of random disorders on the spin-Hall effect has been widely studied over time. The impurities considered have mainly been magnetic^{16–19}, and also static random impurities^{20–29}. Inoue et al.^{30,31} have shown that in a two-dimensional electron gas, spin accumulation can be achieved by applying a bias and have calculated the diffusive conductance tensor. They have also demonstrated that vertex correction in SHC causes SHC to vanish.

In most of the earlier works on spin transport mentioned above, the spin current has been defined in the conventional way and is given by $\frac{\hbar}{4}\{\mathbf{v}, \sigma\}$ ^{13,31}. In the presence of SOIs, this definition suffers from two fundamental drawbacks. First, the conservation of spin magnetic moment no longer holds and secondly, the spin current is found to be finite even in a localized state. To avoid these difficulties, Shi et al.^{32,33} have put forward an alternative definition for the current. They define the current as a time derivative of the polarization operator, which differs from the conventional definition by the torque dipole term. Here the torque dipole term in the case of spin current is given by the expectation value of the rate of change of spin and arises when the spin magnetic moment of the system is not conserved. Recently, we have studied the effect of disorder on the longitudinal charge and spin currents in a 2D system described by the tight-binding model (TBM) incorporating the Rashba SOI (RSOI) effect³⁴. Later we have also studied the same model taking into account the effects of both RSOI and Dresselhaus SOI (DSOI)³⁵. DSOI arises because of the breaking of bulk inversion symmetry and its strength (which is not

¹School of Physics, University of Hyderabad, Hyderabad, Telangana, India. ²Department of Physics, Visva Bharati University, Bolpur, West Bengal, India. ✉email: acsp.uohyd@gmail.com

tunable) is of the same order as RSOI's and is usually present in almost all systems. Therefore, the incorporation of DSOI is important for the proper understanding of any SOI effect.

In this paper, we purport to examine the role of RSOI, DSOI, and the static random disorder on the longitudinal spin conductivity (LSC) and the transverse spin conductivity in a 2D TBM system using Shi's approach. The transverse spin conductivity is usually referred to as the spin Hall conductivity (SHC). For the sake of completeness, we shall also calculate the corresponding charge conductivities. We finally calculate the ratio: SHC/LCC which is known as the spin-Hall angle³⁶ and study its dependence on various parameters.

Model and formalism

We consider a 2D TBM for a system of electrons with RSOI and DSOI^{34,37} in the presence of static impurities which will be considered random. The total Hamiltonian is given by

$$H = H_0 + H_{imp}, \quad (1)$$

with

$$H_0 = \varepsilon_0 \sum_i c_i^\dagger c_i + t \sum_{\langle ij \rangle} [c_i^\dagger c_j + h.c.] - i\alpha_R \sum_{\langle ij \rangle} [c_{ix,iy}^\dagger \sigma^y c_{ix+1,iy} + h.c.] + i\alpha_R \sum_{\langle ij \rangle} [c_{ix,iy}^\dagger \sigma^x c_{ix+1,iy} + h.c.] \\ + i\beta_D \sum_{\langle ij \rangle} [c_{ix,iy}^\dagger \sigma^x c_{ix+1,iy} + h.c.] - \beta_D \sum_{\langle ij \rangle} [c_{ix,iy}^\dagger \sigma^y c_{ix,iy+1} + h.c.], \quad (2)$$

$$H_{imp} = \sum_i \varepsilon_i c_i^\dagger c_i = \sum_i v\delta(R_i - r_l) c_i^\dagger c_i. \quad (3)$$

where $c_i^\dagger = (c_{i\uparrow}^\dagger \ c_{i\downarrow}^\dagger)$, and $c_i = (c_{i\uparrow} \ c_{i\downarrow})$ denote the creation and annihilation operators for the spin up and spin down electrons, ε_0 and t refer respectively to the onsite energy and the hopping integral, $\langle i, j \rangle$ runs over all the nearest neighbors sites, $\sigma^x, \sigma^y, \sigma^z$ are the Pauli matrices, α_R and β_D denote the RSOI and DSOI strengths respectively, R_i and r_l refer to the electron and impurity positions respectively and the electron-impurity strength is measured by v . When $H_{imp} = 0$, the Hamiltonian H can be diagonalized by a unitary transformation and spin degeneracy is lifted by the spin-orbit coupling leading to two non-degenerate states corresponding to two types of electrons. To show this, we perform the transformation:

$$U(\mathbf{k}) \begin{pmatrix} c_{k\uparrow} \\ c_{k\downarrow} \end{pmatrix} = \begin{pmatrix} \alpha_{1,\mathbf{k}} \\ \alpha_{2,\mathbf{k}} \end{pmatrix} = \alpha_{\mathbf{k}}, \quad (4)$$

with

$$U(\mathbf{k}) = \begin{pmatrix} 1 & p_{\mathbf{k}} \\ -p_{\mathbf{k}}^* & 1 \end{pmatrix}, \quad p_{\mathbf{k}} = \zeta(\mathbf{k})/|\zeta|, \quad (4a)$$

and write the Hamiltonian in terms of the new operators as:

$$H_0 = \sum_{\mathbf{k}} [\varepsilon_{1,\mathbf{k}} \alpha_{1,\mathbf{k}}^\dagger \alpha_{1,\mathbf{k}} + \varepsilon_{2,\mathbf{k}} \alpha_{2,\mathbf{k}}^\dagger \alpha_{2,\mathbf{k}}] \quad (5)$$

Energetics of the two types of electrons are given by

$$\varepsilon_{1,2,\mathbf{k}} = \varepsilon_{\mathbf{k}} \pm 2|\zeta(\mathbf{k})|, \quad (6)$$

with

$$\zeta(\mathbf{k}) = (\alpha_R \sin k_y + \beta_D \sin k_x) + i(\alpha_R \sin k_x + \beta_D \sin k_y), \quad \varepsilon_{\mathbf{k}} = \varepsilon_0 + 2t(\cos k_x + \cos k_y). \quad (6a)$$

Relaxation time

The effect of impurity is studied by calculating the relaxation time involved in the scattering of electrons by the impurities. To simplify, we first write the impurity Hamiltonian in terms of the transformed operators $\alpha_{1,\mathbf{k}}$ and $\alpha_{2,\mathbf{k}}$ as

$$H_{imp} = \sum_{\mathbf{k}\mathbf{k}'} [V_{\mathbf{k}\mathbf{k}'}^{11} \alpha_{1,\mathbf{k}}^\dagger \alpha_{1,\mathbf{k}'} + V_{\mathbf{k}\mathbf{k}'}^{12} \alpha_{1,\mathbf{k}}^\dagger \alpha_{2,\mathbf{k}'} + V_{\mathbf{k}\mathbf{k}'}^{21} \alpha_{2,\mathbf{k}}^\dagger \alpha_{1,\mathbf{k}'} + V_{\mathbf{k}\mathbf{k}'}^{22} \alpha_{2,\mathbf{k}}^\dagger \alpha_{2,\mathbf{k}'}], \quad (7)$$

where

$$V_{\mathbf{k}\mathbf{k}'}^{11} = \frac{1}{2N} \sum_l v e^{i(\mathbf{k}-\mathbf{k}') \cdot \mathbf{r}_l} (1 + p_{\mathbf{k}} p_{\mathbf{k}'}^*), \quad V_{\mathbf{k}\mathbf{k}'}^{12} = \frac{1}{2N} \sum_l v e^{i(\mathbf{k}-\mathbf{k}') \cdot \mathbf{r}_l} (p_{\mathbf{k}} - p_{\mathbf{k}'}), \quad (7a)$$

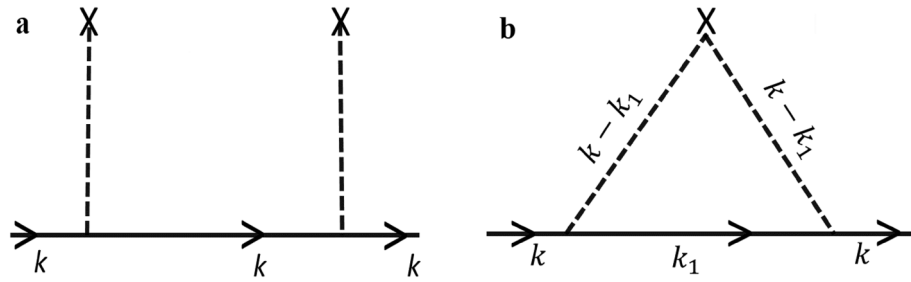


Figure 1. Feynman diagrams for $G(k, ip_n)$ for orders $n=2$.

$$V_{kk'}^{21} = \frac{1}{2N} \sum_l v e^{i(k-k') \cdot r_l} (p_{k'}^* - p_k^*), \quad V_{kk'}^{22} = \frac{1}{2N} (p_{k'}^* - p_k^*) (1 + p_k p_k^*). \tag{7b}$$

In the presence of impurities, the charge carrier will acquire a relaxation time. The relaxation time can be calculated from the imaginary part of the self-energy. The relevant Green function for the electron-impurity system is given by

$$G(k, \tau) = \sum_{l=1}^{\infty} (-1)^l \int_0^{\beta} d\tau_1 \dots \int_0^{\beta} d\tau_n * Tr \left[\alpha_{1,k}^{\dagger}(\tau) V(\tau_1) V(\tau_2) \dots V(\tau_n) \alpha_{1,k}(0) \right] \tag{8}$$

Here we will calculate Green function to the second order, as the first order i.e. $l=1$, give a constant shift in energy. Second order Green function for our Hamiltonian is given by

$$G(k, \tau) = \sum_{k,k'} \int_0^{\beta} \int_0^{\beta} d\tau_1 d\tau_2 \left\langle T_{\tau} \left[\alpha_{1,k} \left(V_{k_1 k_2}^{11} \alpha_{1,k_1}^{\dagger}(\tau_1) \alpha_{1,k_2}(\tau_1) + V_{k_1 k_2}^{12} \alpha_{1,k_1}^{\dagger}(\tau_1) \alpha_{2,k_2}(\tau_1) \right. \right. \right. \\ \left. \left. \left. + V_{k_1 k_2}^{21} \alpha_{2,k_1}^{\dagger}(\tau_1) \alpha_{1,k_2}(\tau_1) + V_{k_1 k_2}^{22} \alpha_{2,k_1}^{\dagger}(\tau_1) \alpha_{2,k_2}(\tau_1) \right) \right. \right. \\ \left. \left. \left(V_{k'_1 k'_2}^{11} \alpha_{1,k'_1}^{\dagger}(\tau_2) \alpha_{1,k'}(\tau_2) + V_{k'_1 k'_2}^{12} \alpha_{1,k'_1}^{\dagger}(\tau_2) \alpha_{2,k'}(\tau_2) \right. \right. \right. \\ \left. \left. \left. + V_{k'_1 k'_2}^{21} \alpha_{2,k'_1}^{\dagger}(\tau_2) \alpha_{1,k'}(\tau_2) + V_{k'_1 k'_2}^{22} \alpha_{2,k'_1}^{\dagger}(\tau_2) \alpha_{2,k'}(\tau_2) \right) \alpha_{1,k}^{\dagger}(0) \right] \right\rangle \tag{9}$$

Using Wick's theorem, the Green function Eq. (9) reduces to

$$G(k, ip_n) = \sum_{k_1} V_{kk_1}^{11} V_{k_1 k}^{11} g^{01}(k, ip_n) g^{01}(k_1, ip_n) g^{01}(k, ip_n) + V_{kk_1}^{12} V_{k_1 k}^{21} g^{01}(k, ip_n) g^{02}(k_1, ip_n) g^{01}(k, ip_n). \tag{10}$$

As the impurities are randomly distributed, we perform impurity averaging over all possible configurations. Considering the distributions of impurities to be uncorrelated in space, we write it as the product of the individual impurity distributions. Since the factor which depends on position is $V_{kk_1} V_{k_1 k}$ and we can write

$$\overline{V_{kk_1} V_{k_1 k}} = \frac{v^2}{4N^2} [(\aleph^2 - \aleph) \delta_{kk_1} \delta_{k_1 k} + \aleph] [(1 + p_k p_{k_1}^*)] [(1 + p_{k_1} p_k^*)] \tag{11}$$

Substituting Eq. (11) in (10) the Green functions reduces to

$$G(k, ip_n) = g^{01}(k, ip_n) \sum_{k_1} \frac{v^2}{4N^2} [(\aleph^2) \delta_{kk_1} \delta_{k_1 k} + \aleph] \times [(1 + p_k p_{k_1}^*)] [(1 + p_{k_1} p_k^*)] \\ \times g^{01}(k_1, ip_n) g^{01}(k, ip_n) + g^{01}(k, ip_n) \times \sum_{k_1} \frac{v^2}{4N^2} [(\aleph^2) \delta_{kk_1} \delta_{k_1 k} + \aleph] \\ \times [(p_k - p_{k_1})] [(p_k^* - p_{k_1}^*)] g^{02}(k_1, ip_n) g^{01}(k, ip_n) \tag{12}$$

In Eq. (12) we have contributions to the Green functions from two terms, one from \aleph and another from \aleph^2 as shown in Fig. 1 where \aleph is the number of impurities present in the system. The contribution from \aleph^2 (Fig. 1a) will be cancelled as it represents a reducible diagram. The contribution from Fig. 1b is given as

$$G(k, ip_n) = g^{01}(k, ip_n) \sum_{k_1} \frac{v^2}{4N} n(1 + p_k p_{k_1}^*) (1 + p_{k_1} p_k^*) g^{01}(k_1, ip_n) \times g^{01}(k, ip_n) + g^{01}(k, ip_n) \sum_{k_1} \frac{v^2}{4N} n(p_k - p_{k_1}) \times (p_k^* - p_{k_1}^*) \times g^{02}(k_1, ip_n) g^{01}(k, ip_n). \tag{13}$$

With further simplification, the Green function equation can be rewritten as

$$G(k, ip_n) = g^{01}(k, ip_n) \Sigma(ip_n) g^{01}(k, ip_n) \tag{14}$$

where $\Sigma(ip_n)$ is the self-energy and is given by

$$\Sigma(ip_n) = \frac{v^2}{4N} \sum_{k_1} [n[(1 + p_k p_{k_1}^*)][(1 + p_{k_1} p_k^*)]] g^{01}(k_1, ip_n) + \frac{v^2}{4N} \sum_{k_1} [n[(p_k - p_{k_1})][(p_k^* - p_{k_1}^*)]] g^{02}(k_1, ip_n). \tag{15}$$

In Eq. (15), $g^{01}(k_1, ip_n)$ and $g^{02}(k_1, ip_n)$ denote the Green functions for an electron in the absence of the impurities and having a particular spin

$$g^{01}(k_1, ip_n) = \sum_{k_1} \frac{1}{ip_n - \epsilon_{1,k_1}}, \quad g^{02}(k_1, ip_n) = \sum_{k_1} \frac{1}{ip_n - \epsilon_{2,k_1}}. \tag{16}$$

The next step is to perform the analytical continuation: $ip_n \rightarrow \epsilon + i\eta$. The self-energy is thus given by

$$\Sigma(\epsilon) = \frac{v^2}{4N} \sum_{k_1} \frac{[n[(1 + p_k p_{k_1}^*)][(1 + p_{k_1} p_k^*)]]}{\epsilon - \epsilon_{1,k_1} + i \text{sgn}(p_n)\eta} + \frac{v^2}{4N} \sum_{k_1} \frac{[n[(p_k - p_{k_1})][(p_k^* - p_{k_1}^*)]]}{\epsilon - \epsilon_{2,k_1} + i \text{sgn}(p_n)\eta}, \tag{17}$$

and the imaginary part of the self-energy gives relaxation time.

$$\frac{1}{\tau_k^{1,2}} = \frac{2\pi}{\hbar} \frac{v^2 n}{4N} \sum_{k_1} \left([(1 + |p_k|^2 |p_{k_1}|^2)] \delta(\epsilon - \epsilon_{1,2,k_1}) + [|p_k|^2 + |p_{k_1}|^2] \delta(\epsilon - \epsilon_{2,1,k_1}) \right) \tag{18}$$

In the dilute-impurity regime, the average-configuration relaxation times for the two types of electrons may be assumed to be equal. Defining a characteristic time scale τ_0 given by: $\tau_0 = \hbar/t$ and introducing: $y'_i = y_i/t, \alpha'_R = \alpha_R/t, \beta'_D = \beta_D/t, v' = v/t, \mu' = \mu/t, \epsilon'_0 = \epsilon_0/t$, we finally obtain:

$$\left(\frac{\tau}{\tau_0} \right)^{-1} = \frac{v'^2 n_{imp}}{2\pi} \times \int_0^\pi dk_x \sum_{i=1,2} \left((h'_1(k_x, y_i))^{-1} + (h'_2(k_x, y_i))^{-1} \right) (z'_i)^{-1}, \tag{19}$$

where y'_i is given by

$$y'_i = \frac{\mu' - 2\cos k_x \pm 2\sqrt{\mathbb{C}}}{1 + (\alpha'^2_R + \beta'^2_D + 2\alpha'_R \beta'_D \sin k_x)}, \quad \mathbb{C} = (\alpha'^2_R + \beta'^2_D) \sin^2 k_x + \alpha'^2_R + \beta'^2_D + 4\alpha'_R \beta'_D$$

$$z'_i = (1 - y'^2_i/4)^{1/2}, h'_{1,2}(k_x, y_i) = 1/\mathbb{Z}, \quad \mathbb{Z} = \frac{y'_i (2\alpha'_R \beta'_D \sin k_x + (\alpha'^2_R + \beta'^2_D) z'_i)}{8z'^2_i [(\alpha'_R \sin k_x + \beta'_D z'_i)^2 + (\alpha'_R z'_i + \beta'_D \sin k_x)^2]^{1/2}} \tag{20}$$

(a) Charge current

When SOs are present, the charge current operators J^c can be obtained by differentiating the charge polarization operator with respect to time: $\mathbf{P}^c = e \sum_{j_x, j_y} \mathbf{R}_{j_x, j_y} c^\dagger_{j_x, j_y} I_{c_{j_x, j_y}}$ where \mathbf{R}_{j_x, j_y} denotes the position observable. Here we work in the Heisenberg picture to calculate the currents. The charge current along the x and y axis is given in terms of the transformed operators as:

$$J^c_{x,y} = \frac{\partial \mathbf{P}^c}{\partial t} = i \left[H_0, e \sum_{j_x, j_y} \vec{R}_{j_x, j_y} c^\dagger_{j_x, j_y} I_{c_{j_x, j_y}} \right] \tag{21}$$

which can be written as

$$J^c_{x,y} = e/\hbar \sum_k \left(f_1^{x,y}(\mathbf{k}) \alpha^\dagger_{1,k} \alpha_{1,k} + f_2^{x,y}(\mathbf{k}) \alpha^\dagger_{2,k} \alpha_{2,k} + f_3^{x,y}(\mathbf{k}) \alpha^\dagger_{1,k} \alpha_{2,k} + f_3^{*x,y}(\mathbf{k}) \alpha^\dagger_{1,k} \alpha_{2,k} \right), \tag{22}$$

where

$$f_{1,2}^x(\mathbf{k}) = 2tsink_x \mp \cos k_x \left(i\alpha_R \left(p_{k_x,k_y}^* - p_{k_x,k_y} \right) + h_D \left(p_{k_x,k_y}^* + p_{k_x,k_y} \right) \right), \tag{22a}$$

$$f_{1,2}^y(\mathbf{k}) = 2tsink_y \mp \cos k_x \left(i\alpha_R \left(p_{k_x,k_y}^* - p_{k_x,k_y} \right) + h_D \left(p_{k_x,k_y}^* + p_{k_x,k_y} \right) \right), \tag{22b}$$

$$f_3^x(\mathbf{k}) = -\cos k_x \left(i\alpha_R \left(1 + p_{k_x,k_y}^2 \right) + \beta_D \left(1 - p_{k_x,k_y}^2 \right) \right), \tag{22c}$$

$$f_3^y(\mathbf{k}) = -\cos k_y \left(i\alpha_R \left(1 + p_{k_x,k_y}^2 \right) + \beta_D \left(1 - p_{k_x,k_y}^2 \right) \right), \tag{22d}$$

(b) Spin current. Similarly, to calculate the spin current density, we define spin polarization operator $\mathbf{P}^{sz} = \sum_{j_x,j_y} \mathbf{R}_{j_x,j_y} s_z c_{j_x,j_y}^\dagger c_{j_x,j_y}$, and the spin current is given by

$$J_x^{sz} = \frac{dP^{sz}}{dt} = \frac{i}{\hbar} [P^{sz}, H_0], = \sum_{j_x,j_y} \mathbf{R}_{j_x,j_y} \frac{ds_z}{dt} \tag{23}$$

where $\frac{ds_z}{dt} \equiv \hat{\tau} = \frac{1}{i\hbar} [\hat{s}_z, H_0]$, $\hat{\tau}$ being related to the spin torque density T_z through the relation: $T_z = \psi^\dagger(\mathbf{r}) \hat{\tau} \psi(\mathbf{r})$. So the spin current is zero if the spin torque density is zero. Thus spin current introduced here arises from the spin torque caused by the spin-orbit interaction. To calculate the spin current we have used relation (23). Therefore, the x-component of the spin current in terms of operators α_k and α_k^\dagger can be written as:

$$\begin{aligned} J_x^{sz} = & -2t \sum_{k_x,k_y} \sin k_x (\alpha_R \sin k_y + \beta_D \sin k_x) \frac{1}{|\zeta(\mathbf{k})|} \alpha_k^\dagger \sigma_x \alpha_k \\ & + 2t \sum_{k_x,k_y} \sin k_x (\alpha_R \sin k_x + \beta_D \sin k_y) |\zeta(\mathbf{k})|^{-1} \alpha_k^\dagger \sigma_y \alpha_k \\ & + 2 \sum_{k_x,k_y} (\beta_D^2 - \alpha_R^2) \cos k_x \sin^2 k_y |\zeta(\mathbf{k})|^{-2} \\ & \times \alpha_k^\dagger \begin{bmatrix} (\beta_D - i\alpha_R) p_{k_x,k_y}^* & (\beta_D + i\alpha_R) p_{k_x,k_y}^2 \\ -(\beta_D - i\alpha_R) p_{k_x,k_y}^{*2} & (\beta_D + i\alpha_R) p_{k_x,k_y} \end{bmatrix} \alpha_k. \end{aligned} \tag{24}$$

Spin hall and charge conductivity

Next, to study the effect of Rashba and Dresselhaus SOIs and the static random impurities on the currents, we employ the Green function formalism of Kubo^{38,39}. In this technique, the longitudinal charge conductivity is obtained from the imaginary part of the charge current-current correlation function

$$\prod_c(i\omega_n) = \frac{\hbar}{N} \int_0^\beta d\tau e^{i\omega_n\tau} \langle T_\tau J^{cx}(\tau) J^{cx}(\tau') \rangle. \tag{25}$$

Conductivity is calculated using imaginary part of $\prod(i\omega)$.

$$\sigma_{xx} = \lim_{\omega \rightarrow 0} \text{Im} \left[\frac{\prod_c(i\omega_n)}{\omega} \right]. \tag{26}$$

where ω_n represent the Matsubara frequency, T_τ is the imaginary time ordering, $\beta = 1/\kappa_B T$ is the Boltzmann factor, the brackets ... represent the thermodynamic average and N is the number of lattice sites. The charge current at two different times can be obtained from Eq. (21) as

$$\begin{aligned} \vec{J}_x^c(\tau) = & \sum_k \left(f_1^x(k) \alpha_{1,k}^\dagger(\tau) \alpha_{1,k}(\tau) + f_2^x(k) \alpha_{2,k}^\dagger(\tau) \alpha_{2,k}(\tau) \right. \\ & \left. + f_3^x(k) \alpha_{1,k}^\dagger(\tau) \alpha_{2,k}(\tau) + f_3^{*x}(k) \alpha_{1,k}^\dagger(\tau) \alpha_{2,k}(\tau) \right) \end{aligned} \tag{27}$$

$$\begin{aligned} \vec{J}_x^c(\tau') = & \sum_k \left(f_1^x(k) \alpha_{1,k}^\dagger(\tau') \alpha_{1,k}(\tau') + f_2^x(k) \alpha_{2,k}^\dagger(\tau') \alpha_{2,k}(\tau') \right. \\ & \left. + f_3^x(k) \alpha_{1,k}^\dagger(\tau') \alpha_{2,k}(\tau') + f_3^{*x}(k) \alpha_{1,k}^\dagger(\tau') \alpha_{2,k}(\tau') \right) \end{aligned} \tag{28}$$

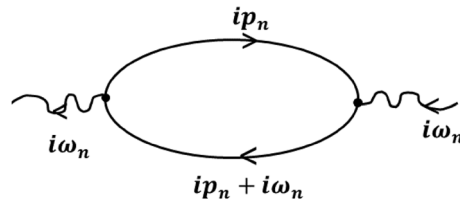


Figure 2. Bubble diagram for the current–current correlation function.

The expression for the current–current correlation function is calculated by substituting Eqs. (27) and (28) in Eq. (25):

$$\begin{aligned} \prod_c (i\omega_n) = & \frac{\hbar}{N} \int_0^\beta d\tau e^{i\omega\tau} \left\langle \left[\sum_k f_1^x(k)^2 \alpha_{1,k}^\dagger(\tau) \alpha_{1,k}(\tau) \alpha_{1,k}^\dagger(\tau') \alpha_{1,k}(\tau') \right. \right. \\ & + \sum_k f_2^x(k)^2 \alpha_{2,k}^\dagger(\tau) \alpha_{2,k}(\tau) \alpha_{2,k}^\dagger(\tau') \alpha_{2,k}(\tau') \\ & + \sum_k f_3^x(k) f_3^{x*}(k) \alpha_{1,k}^\dagger(\tau) \alpha_{2,k}(\tau) \alpha_{2,k}^\dagger(\tau') \alpha_{1,k}(\tau') \\ & \left. \left. + \sum_k f_3^x(k) f_3^{x*}(k) \alpha_{2,k}^\dagger(\tau) \alpha_{1,k}(\tau) \alpha_{1,k}^\dagger(\tau') \alpha_{2,k}(\tau') \right] \right\rangle \end{aligned} \tag{29}$$

Equation (29) is solved in parts. We first calculate the correlation function corresponding to the first term of Eq. (29). Using Wick’s theorem, the current–current correlation function for the first term in the Fourier basis is given by:

$$\prod_c (i\omega_n) = \frac{\hbar}{N} \frac{1}{\beta} \sum_{k, ip_n} f_1^x(k)^2 \int_0^\beta d\tau G(k, ip_n) G(k, ip_n + i\omega_n), \tag{30}$$

where $G(k, ip_n)$ and $G(k, ip_n + i\omega_n)$ are the single particle Green functions which are represented by the lower and upper lines of the loop of the bubble diagram for the current–current correlation function shown in Fig. 2. It can be seen that at the vertices where the electrons lines meet, the momentum is conserved. Here the two electron lines differ by the Matsubara frequency $i\omega_n$. In order to calculate the charge conductivity (CC) we calculate the imaginary part of the current–current correlation function and perform analytic continuation ($i\omega_n \rightarrow \omega + i\delta$) and write the Green functions in terms of spectral functions. Finally, we divide the correlation function by ω and in the limit $\omega \rightarrow 0$, CC for the first part of current–current correlation function is given by

$$\sigma_{xx}^c = -\frac{\hbar}{N} \sum_k f_1^x(k)^2 \int_{-\infty}^\infty d\epsilon A(k, \epsilon)^2 \left\{ \frac{\partial n_F(\epsilon)}{\partial \epsilon} \right\}. \tag{31}$$

Similarly, we can evaluate correlation functions for the other terms of Eq. (29) and the total CC assumes the following expression:

$$\sigma_{xx}^c = -\frac{\hbar}{N} \sum_k \int d\epsilon \left\{ \frac{\partial n_F(\epsilon)}{\partial \epsilon} \right\} [f_1^{x2}(k) A^1(k, \epsilon)^2 + f_2^{x2}(k) A^2(k, \epsilon)^2 + 2f_3^{x2} A^1(k, \epsilon) A^2(k, \epsilon)], \tag{32}$$

where $A^1(k, \epsilon)$ and $A^2(k, \epsilon)$ represent the spectral functions for the electrons. In the case of low impurity concentration, the spectral function is given by:

$$(A^{1,2}(k, \epsilon))^2 = (4\pi/\hbar) \tau(\mathbf{k}, \mu) \delta(\mu - \epsilon_{k1,2}). \tag{33}$$

Using Eq. (33) in Eq. (32), the expression for longitudinal CC reduces to

$$\sigma_{xx}^c = \frac{4\pi e^2 \tau}{\hbar \tau_0 k T'} \iint_{-\pi}^\pi dk_x dk_y \sum_{i=1,2} \left((f'_{ix}(k_x, y_i))^2 \times \exp \left(\frac{(\epsilon'_{i,k} - \mu')/kT'}{1 + \exp \left(\frac{(\epsilon'_{i,k} - \mu')/kT'}{kT'} \right)} \right)^2 \right), \tag{34}$$

Similarly, from the Kubo formalism, the expression for the spin Hall conductivity (SHC) is given by

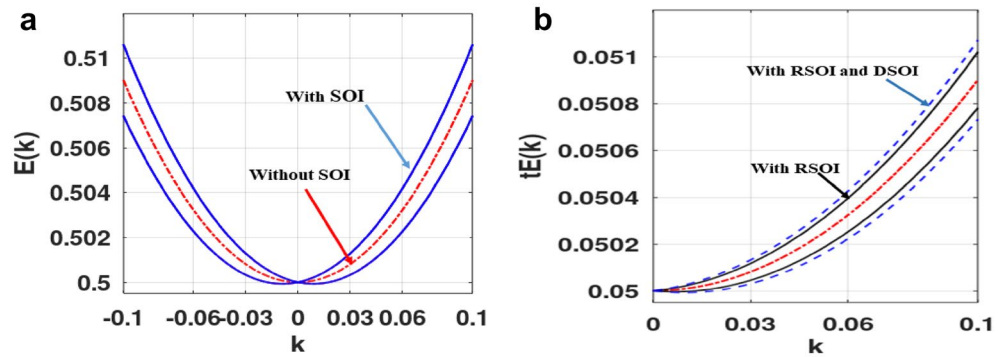


Figure 3. (a) Energy dispersion along the x-direction in k space. (b) For different values of α_R and β_D . (Plotted using octave–6.3.0).

$$\sigma_{xy}^{sz} = -\frac{1}{\pi} \sum \frac{\text{Im}[\langle J_x^{sz} | \rangle \langle J_y^c | \rangle]}{(\epsilon_{1,k} - \epsilon_{2,k})^2 + (\frac{1}{\tau})^2} (f_E(\epsilon_{1,k} - \mu') - f_E(\epsilon_{2,k} - \mu')), \tag{35}$$

where J_x^{sz} is the x-component of the spin current and J_y^c is the y-component of charge current. Using the value of J_x^{sz} and J_y^c from Eqs. (22) and (23), the final expression for SHC is given by

$$\sigma_{xy}^{sz} = \frac{(\alpha'_R)^2 - \beta'_D)^2}{\pi} \times \int_0^\pi \int_0^\pi dk_x dk_y \frac{(f_E(\epsilon_{1,k} - \mu') - f_E(\epsilon_{2,k} - \mu')) \cos k_y \sin^2 k_x}{((\zeta'(k))^2 + (\tau_0/\tau)^2)(\zeta'(k))}, \tag{36}$$

where $f_E(\epsilon_{1,2,k} - \mu')$ is the Fermi distribution and at zero temp it is given by $f_E(\epsilon_{1,2,k} - \mu') = \text{heavieside}(\epsilon_k \pm 2|\zeta(k) - \mu')$.

Numerical results discussion

We measure all energies in units of t . Numerical computations have been done using the software GNU Octave version 6.3.0⁴⁰. Figure 3 shows the energy dispersion along the k_x -direction in the presence and absence of SOI. The splitting of bands and the renormalization of the ground state energy (GS) are clearly visible.

The effect of this splitting and the renormalization can be seen in Fig. 4, where SHC is plotted with respect to chemical potential. Initially SHC increases with μ (Fig. 4a), reaches a maximum at some crucial μ -value and then decreases with a further increase in μ to zero (Fig. 4b). When studied in the presence of the DSOI (Fig. 4a), SHC increases with μ at a lower rate as it counters the Rashba effect. This increase in SHC with chemical potential can be easily understood from Fig. 5. At low μ , the density of states is high which gives rise to more scattering events leading to a lower value in SHC. As μ increases, DOS decreases and we observe an increase in SHC. However, as μ increases beyond a certain value, DOS becomes very small (Fig. 5), and then not any states are available for conduction and SHC decreases with μ at large value of μ (Fig. 4b). As a result, SHC exhibits a maximum with respect to μ (Fig. 4b). Figure 4c shows the nature of the variation of SHC with respect to μ for different values of the impurity strength (v). As expected, with an increase in impurity strength, SHC decreases.

In Fig. 6, we present the behaviour of SHC as a function of α_R with different values of SMT parameters. Figure 6a describes the behavior of SHC versus RSOI strength α_R . One can see that at $\beta_D = 0$, SHC is zero up to a certain value of α_R . For $\beta_D \neq 0$, SHC has a finite value finite at $\alpha_R = 0$. This shows that the difference in the spin states is minimum at smaller value of α_R for $\beta_D = 0$, while for finite β_D , there is an appreciable difference in the spin states that causes a larger spin current. As α_R increases, RSOI counters the effect of DSOI and concomitantly, SHC decreases. SHC becomes zero when α_R becomes equal to β_D . As α_R increases further, SHC increases with α_R (Fig. 6a). With the increase in α_R beyond $\alpha_R = \beta_D$, the spin up and down bands move apart, causing a higher spin imbalance and hence a rise in SHC. As α_R is increased further, SHC exhibits an asymmetric peak at a critical α_R , and then decreases with further increase in α_R and finally reaches a constant saturation value (Fig. 6b). This peak mentioned above gives the maximum value of SHC for the system. As β_D is increased, the spin imbalance decreases leading to a decrease in spin current. Figure 6c displays the behaviour of SHC as a function of α_R for a few values of μ . The plot exhibits a similar nature as in Fig. 6a. SHC increases with the increase in μ , which is also evident from Fig. 4. In Fig. 6d we examine the behaviour of SHC versus α_R for different values of the impurity strength. The figure shows that as the impurity strength increases, SHC decreases. In Fig. 7, SHC is considered as a function of impurity strength for various system parameters. When the strength of impurity scattering coefficient is very small, SHC remains essentially unaffected by impurity. As the impurity coupling increases, one can observe a gradual decrease in SHC. Figure 7a,b shows that with an increase in DSOI strength and chemical potential, SHC has a lower value and higher decreasing rate.

Finally In the last segment, we present our results for the spin-Hall angle (SHA) which is measured by the ratio: SHC/LCC. The effect of RSOI, DSOI and the impurity on LCC was thoroughly investigated by us in our earlier works^{34,35}. Figure 8a,b shows the plot of SHA versus α_R for different values of the chemical potential and

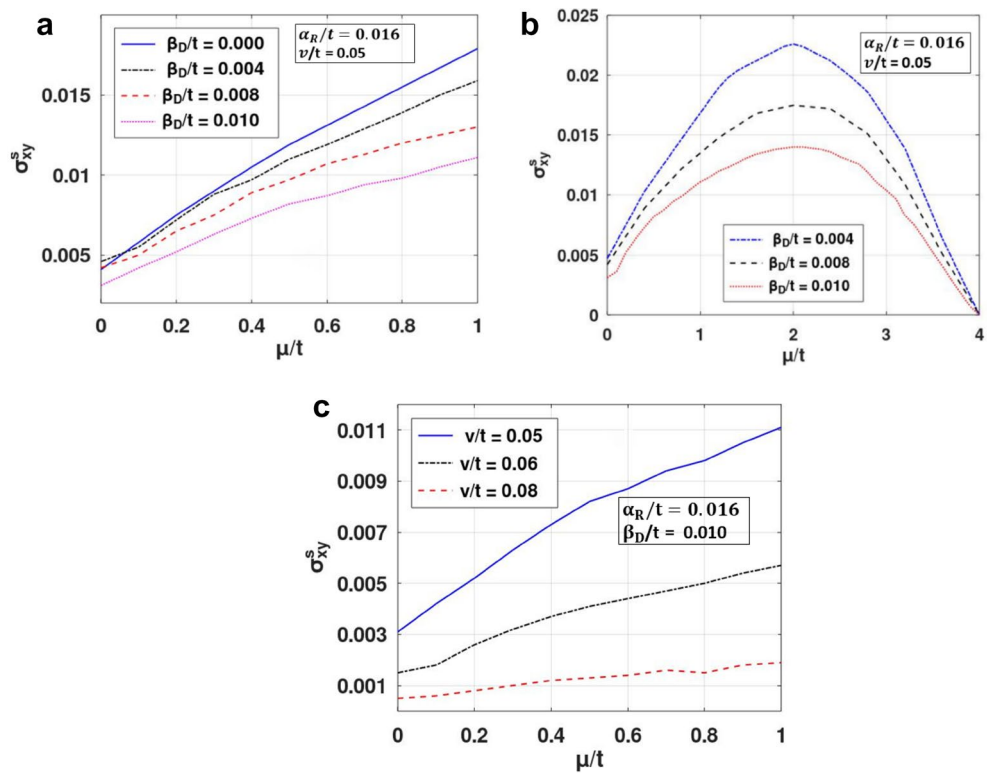


Figure 4. SHC versus μ/t for different values of: (a, b) β'_D , (c) v' . (Plotted using octave – 6.3.0).

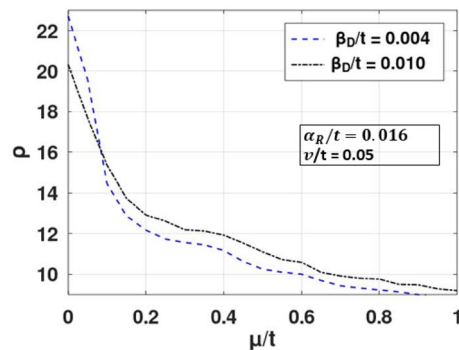


Figure 5. Density of state (ρ) vs μ/t . (Plotted using octave – 6.3.0).

impurity strength. SHC increase with increase in chemical potential while decrease with increase in impurity strength similar to SHC. And for higher value of Rashba strength once again one can observe a peak-like structure, which is maximum for a lower value of β_D (Fig. 8c).

In Fig. 9, we show the three-dimensional and contour plots for the ratio of the spin Hall to charge conductivities as a function of α_R and β_D . As anticipated, when α_R and β_D are small, the ratio of SHC to LCC is almost zero. As we increase any one of the SOI strengths (keeping the other constant), the ratios initially increase but beyond a critical value of α_R or β_D they decrease. This gives rise to peak structures in SHC/LCC. When α_R and β_D are both increased together, the ratio remains zero, and as one becomes more effective than the other, we witness a measurable value. The Rashba strength can be adjusted up to 50% by varying the gate voltage^{41–43}. Figure 10 shows the SHC/LCC ratio for Indium arsenide for which α_R and β_D can take values in the range: 0.07–1.6 meV and μ can be in the range: 20–50 meV^{39,44}. It can be seen that when impurity strength is low, SHA increases. This is because at low impurity concentration, SHC remains constant (Fig. 7) while LCC decreases³⁵. From Fig. 10, one can see that for InAs, SHA can be in the range: 0.00001–0.00015.

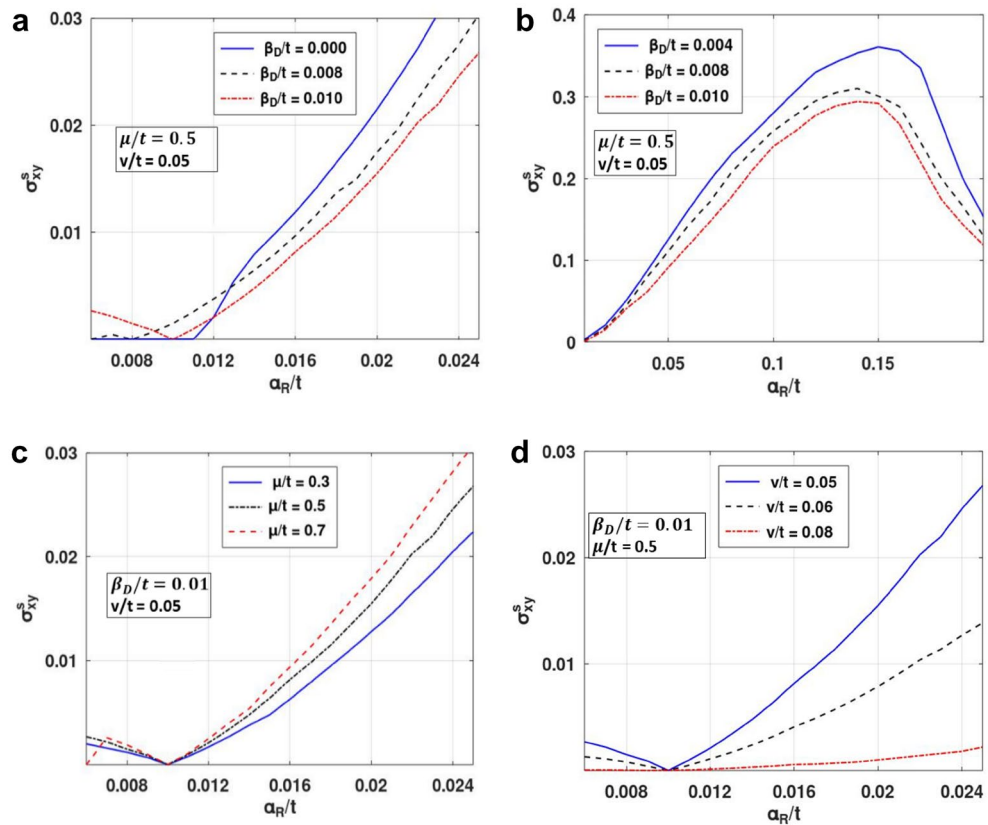


Figure 6. SHC versus α_R/t for different value of: (a, b) β_D/t , (c) μ/t and (d) ν/t . (Plotted using octave – 6.3.0).

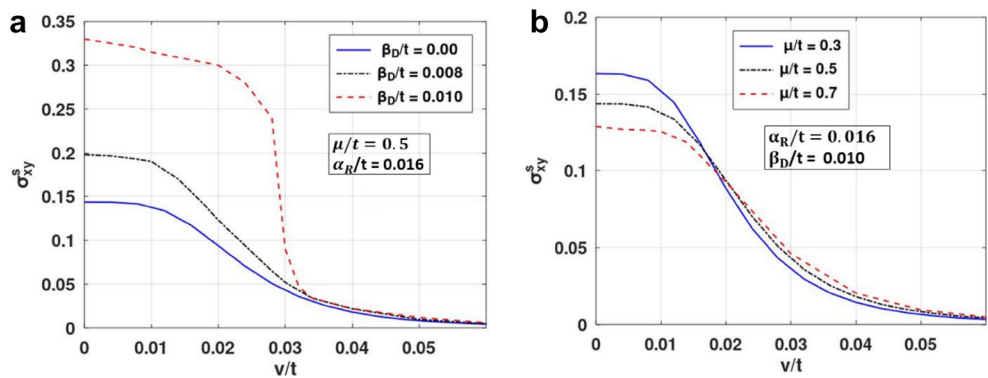


Figure 7. SHC versus ν/t for distinct: (a) β_D/t , and (b) μ/t values. (Plotted using octave – 6.4.0).

Conclusion

We have explored the nature of spin-torque-induced transport properties of a two-dimensional tight-binding system in the presence of Rashba and Dresselhaus spin-orbit interactions and random static impurities. In the absence of impurity scattering, the system admits an exact solution with two degenerate electron states. We have treated the electron-impurity scattering by the Matsubara Green function technique using the diagrammatic perturbation theory. The randomness of the impurities has been taken into account by performing configuration averaging. Finally, the Kubo formalism is used to calculate spin-Hall conductivity.

Our results suggest that as a function of the chemical potential, the spin-Hall conductivity increases monotonically for the smaller values has a peak structure for higher values. The peak values of these quantities, however

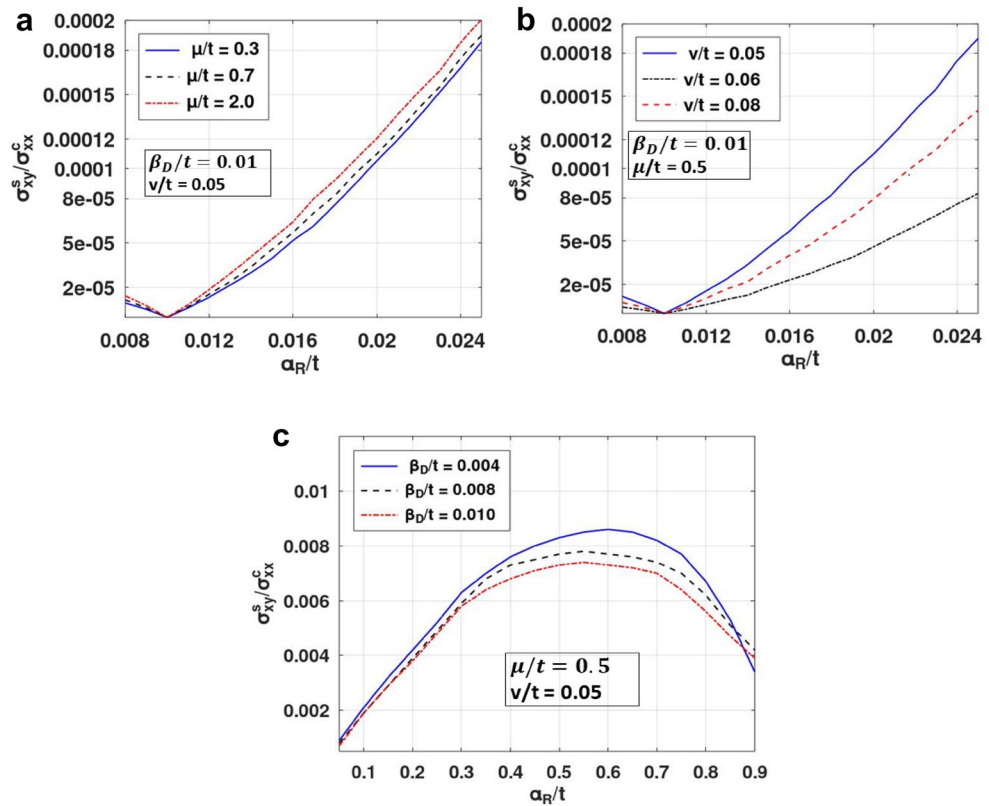


Figure 8. SHA versus RSOI coefficient for different value of: (a) μ/t , (b) v/t and (c) β_D/t . (Plotted using octave – 6.3.0).

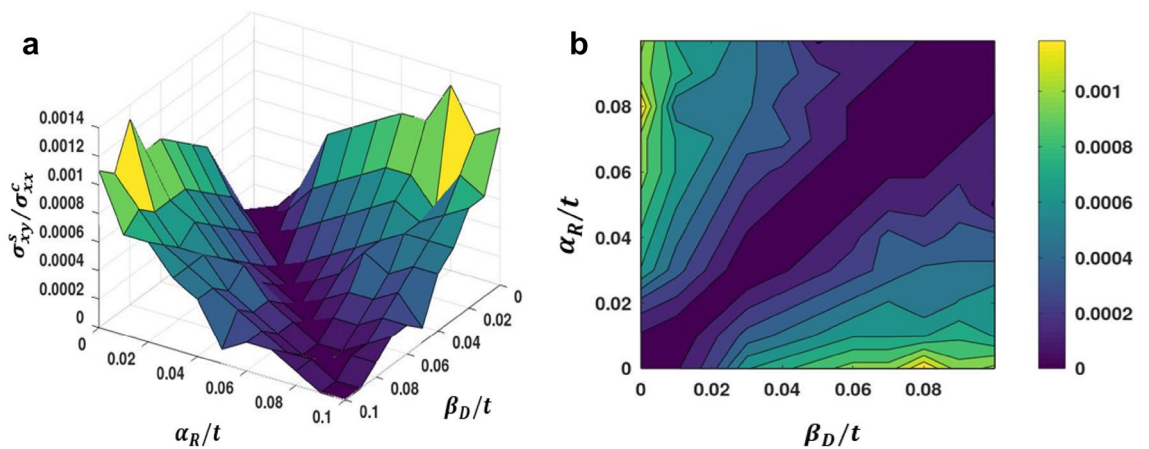


Figure 9. (a) SHC/LCC as a function of α_R/t and β_D/t . (b) Contour plot of SHC/LCC in the $(\alpha_R - \beta_D)$ –plane for $\mu/t=0.05$ and $v/t=0.05$. (Plotted using octave – 6.3.0).

decrease with the increase in the Dresselhaus coupling, as the DSOI broadens the bands. Similar nature is also observed with respect to the RSOI coefficient.

We have also studied the effect of the electron-impurity interaction strength v on SHC in the presence of both the RSOI and DSOI effects and observed that for low impurity strength, SHC remains almost negligible, but with an increase in the impurity strength, SHC decreases rapidly and the rate of decrease depends on the difference between α_R and β_D .

Finally, the spin-Hall angle has been calculated and it is shown that when one of the two spin-orbit interactions dominates, the spin-Hall angle increases and it vanishes whenever the Rashba and Dresselhaus interactions become equal. As an example, the variation of SHA as a function of the impurity coupling strength is shown for InAs.

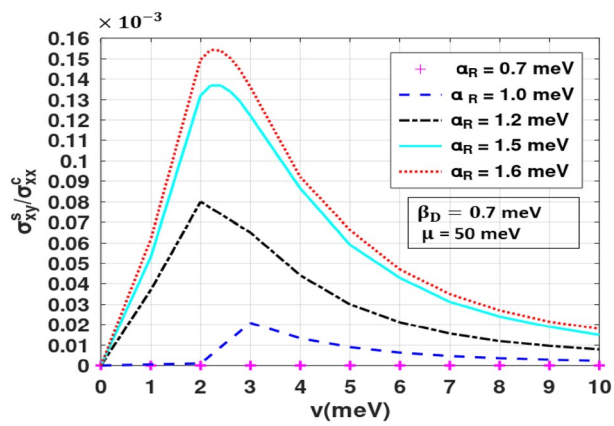


Figure 10. SHC/LCC as a function of ν . (Plotted using octave – 6.3.0).

Received: 28 August 2021; Accepted: 4 August 2022

Published online: 20 August 2022

References

- Wolf, S. A. *et al.* Spintronics: A spin-based electronics vision for the future. *Science* **294**, 14882 (2001).
- Prinz, G. A. Magneto-electronics. *Science* **282**, 1660 (1998).
- Jedema, F. J., Nijboer, M. S., Filip, T. & Van Wees, B. J. Spin injection and spin accumulation in all-metal mesoscopic spin valves. *Phys. Rev. B* **67**, 085319 (2003).
- Ji, Y., Hoffmann, A., Jiang, J. S. & Bader, S. D. Spin injection, diffusion, and detection in lateral spin-valves. *Appl. Phys. Lett.* **85**, 6218 (2004).
- Kimura, T., Hamrle, J. & Otani, Y. Estimation of spin-diffusion length from the magnitude of spin-current absorption: Multiterminal ferromagnetic/nonferromagnetic hybrid structures. *Phys. Rev. B* **72**, 014461 (2005).
- Ku, J., Chang, J., Han, S., Ha, J. & Eom, J. Electrical spin injection and accumulation in ferromagnetic/Au/ferromagnetic lateral spin valves. *J. Appl. Phys.* **99**, 08H705 (2006).
- Laczkowski, P. Enhancement of the spin signal in permalloy/gold multiterminal nanodevices by lateral confinement. *Phys. Rev. B* **85**, 220404 (2012).
- Villamor, E., Isasa, M., Hueso, L. E. & Casanova, F. Contribution of defects to the spin relaxation in copper nanowires. *Phys. Rev. B* **87**, 094417 (2013).
- Villamor, E., Isasa, M., Hueso, L. E. & Casanova, F. Temperature dependence of spin polarization in ferromagnetic metals using lateral spin valves. *Phys. Rev. B* **88**, 184411 (2013).
- Saitoh, E., Ueda, M., Mikajima, H. & Tataru, G. Conversion of spin current into charge current at room temperature: Inverse spin-Hall effect. *Appl. Phys. Lett.* **88**, 182509 (2006).
- Sharma, P. & Brouwer, P. W. Mesoscopic effects in adiabatic spin pumping. *Phys. Rev. Lett.* **91**, 166801 (2003).
- Murakami, S., Nagaosa, N. & Zhang, S. C. Dissipationless quantum spin current at room temperature. *Science* **301**, 1348 (2003).
- Sinova, J. *et al.* Universal intrinsic spin hall effect. *Phys. Rev. Lett.* **92**, 126603 (2004).
- Hirsch, J. E. Spin hall effect. *Phys. Rev. Lett.* **83**, 1834 (1999).
- Zhang, S. Spin hall effect in the presence of spin diffusion. *Phys. Rev. Lett.* **83**, 393 (2000).
- Zarea, M. & Ulloa, S. E. Spin Hall effect in two-dimensional p-type semiconductors in a magnetic field. *Phys. Rev. B* **73**, 165306 (2006).
- Wang, P., Li, Y.-Q. & Zhao, X. Nonvanishing spin Hall currents in the presence of magnetic impurities. *Phys. Rev. B* **75**, 075326 (2007).
- van den Berg, T. L., Raymond, L. & Verga, A. Dynamical spin Hall conductivity in a magnetic disordered system. *Phys. Rev. B* **84**, 245210 (2011).
- Gorini, C. *et al.* Theory of current-induced spin polarization in an electron gas. *Phys. Rev. B* **95**, 205424 (2017).
- Schliemann, J. & Loss, D. Anisotropic transport in a two-dimensional electron gas in the presence of spin-orbit coupling. *Phys. Rev. B* **68**, 165311 (2003).
- Popp, M., Frustaglia, D. & Richter, K. Conditions for adiabatic spin transport in disordered systems. *Phys. Rev. B* **68**, 041303 (2003).
- Sheng, L., Sheng, D. N. & Ting, C. S. Spin-hall effect in two-dimensional electron systems with Rashba spin-orbit coupling and disorder. *Phys. Rev. Lett.* **94**, 016602 (2005).
- Raimondi, R. & Schwab, P. Spin-Hall effect in a disordered two-dimensional electron system. *Phys. Rev. B* **71**, 033311 (2005).
- Dugaev, V. K., Inglot, M., Sherman, E. Y. & Barnaś, J. Robust impurity-scattering spin Hall effect in a two-dimensional electron gas. *Phys. Rev. B* **82**, 121310 (2010).
- Mishchenko, E. G., Shtyov, A. V. & Halperin, B. I. Spin current and polarization in impure two-dimensional electron systems with spin-orbit coupling. *Phys. Rev. Lett.* **93**, 226602 (2004).
- Chalaev, O. & Loss, D. Spin-Hall conductivity due to Rashba spin-orbit interaction in disordered systems. *Phys. Rev. B* **71**, 245318 (2005).
- Dimitrova, O. V. Spin-Hall conductivity in a two-dimensional Rashba electron gas. *Phys. Rev. B* **71**, 245327 (2005).
- Onoda, M. & Nagaosa, N. Role of relaxation in the spin Hall effect. *Phys. Rev. B* **72**, 081301 (2005).
- Adagideli, I. & Bauer, G. E. W. Intrinsic spin Hall edges. *Phys. Rev. Lett.* **95**, 256602 (2005).
- Inoue, J. I., Bauer, G. E. W. & Molenkamp, L. W. Diffuse transport and spin accumulation in a Rashba two-dimensional electron gas. *Phys. Rev. B* **67**, 033104 (2003).
- Inoue, J. I., Bauer, G. E. W. & Molenkamp, L. W. Suppression of the persistent spin Hall current by defect scattering. *Phys. Rev. B* **70**, 041303 (2004).
- Shi, J., Zhang, P., Xiao, D. & Niu, Q. Proper definition of spin current in spin-orbit coupled systems. *Phys. Rev. Lett.* **96**, 076604 (2006).
- Zhang, P., Wang, Z., Shi, J., Xiao, D. & Niu, Q. Theory of conserved spin current and its application to a two-dimensional hole gas. *Phys. Rev. B* **77**, 075304 (2008).
- Sharma, H., Sil, S. & Chatterjee, A. Spin torque induced spin current in a two-dimensional tight-binding system with Rashba coupling in the presence of random impurities. *J. Magn. Magn. Mater.* **500**, 166329 (2020).
- Sharma, H. K., Sil, S. & Chatterjee, A. Spin transport in a two-dimensional tight-binding system with Rashba and Dresselhaus spin-orbit interactions in the presence of static random disorder. *J. Magn. Magn. Mater.* **529**, 167711 (2021).
- Dyakonov, M. I. & Khaetskii, A. V. Spin physics in semiconductor. In *Spin Physics in Semiconductors* (ed. Dyakonov, M. I.) 212 (Springer, 2008).
- Rashba, E. I. Spin currents in thermodynamic equilibrium: The challenge of discerning transport currents. *Phys. Rev. B* **68**, 241315 (2003).
- Mahan, G. D. *Many Particle Physics* (Plenum, 1981).
- Sinityn, N. A., Hankiewicz, E. M., Teizer, W. & Sinova, J. Spin Hall and spin-diagonal conductivity in the presence of Rashba and Dresselhaus spin-orbit coupling. *Phys. Rev. B* **70**, 081312 (2004).
- Eaton, J. W., Bateman, D., Hauberg, S. & Wehbring, R. GNU Octave Version 6.3.0 Manual: A High-Level Interactive Language for Numerical Computations, CreateSpace Independent Publishing Platform (2014). ISBN 1441413006, <http://www.gnu.org/software/octave/doc/interpreter/>
- Miller, J. B. *et al.* Gate-controlled spin-orbit quantum interference effects in lateral transport. *Phys. Rev. Lett.* **90**, 076807 (2003).
- Nitta, J., Akazaki, T., Takayanagi, H. & Enoki, T. Gate control of spin-orbit interaction in an inverted $\text{In}_{0.53}\text{Ga}_{0.47}\text{As}/\text{In}_{0.52}\text{Al}_{0.48}\text{As}$ heterostructure. *Phys. Rev. Lett.* **78**, 1335 (1997).
- Ganichev, S. D. *et al.* Experimental separation of Rashba and Dresselhaus spin-splittings in semiconductor quantum wells. *cond-mat/0306521* (2003).
- Kulish, V., Liu, W. & Manzhos, S. A model for estimating chemical potentials in ternary semiconductor compounds: The case of InGaAs. *MRS Adv.* **1**, 2909–2914 (2017).

Author contributions

H.K.S. and S.S. performed the calculation. H.K.S. did the numerical computation and wrote the draft manuscript. A.C. reviewed the manuscript and supervised the work.

Competing interests

The authors declare no competing interests.

Additional information

Correspondence and requests for materials should be addressed to A.C.

Reprints and permissions information is available at www.nature.com/reprints.

Publisher's note Springer Nature remains neutral with regard to jurisdictional claims in published maps and institutional affiliations.



Open Access This article is licensed under a Creative Commons Attribution 4.0 International License, which permits use, sharing, adaptation, distribution and reproduction in any medium or format, as long as you give appropriate credit to the original author(s) and the source, provide a link to the Creative Commons licence, and indicate if changes were made. The images or other third party material in this article are included in the article's Creative Commons licence, unless indicated otherwise in a credit line to the material. If material is not included in the article's Creative Commons licence and your intended use is not permitted by statutory regulation or exceeds the permitted use, you will need to obtain permission directly from the copyright holder. To view a copy of this licence, visit <http://creativecommons.org/licenses/by/4.0/>.

© The Author(s) 2022